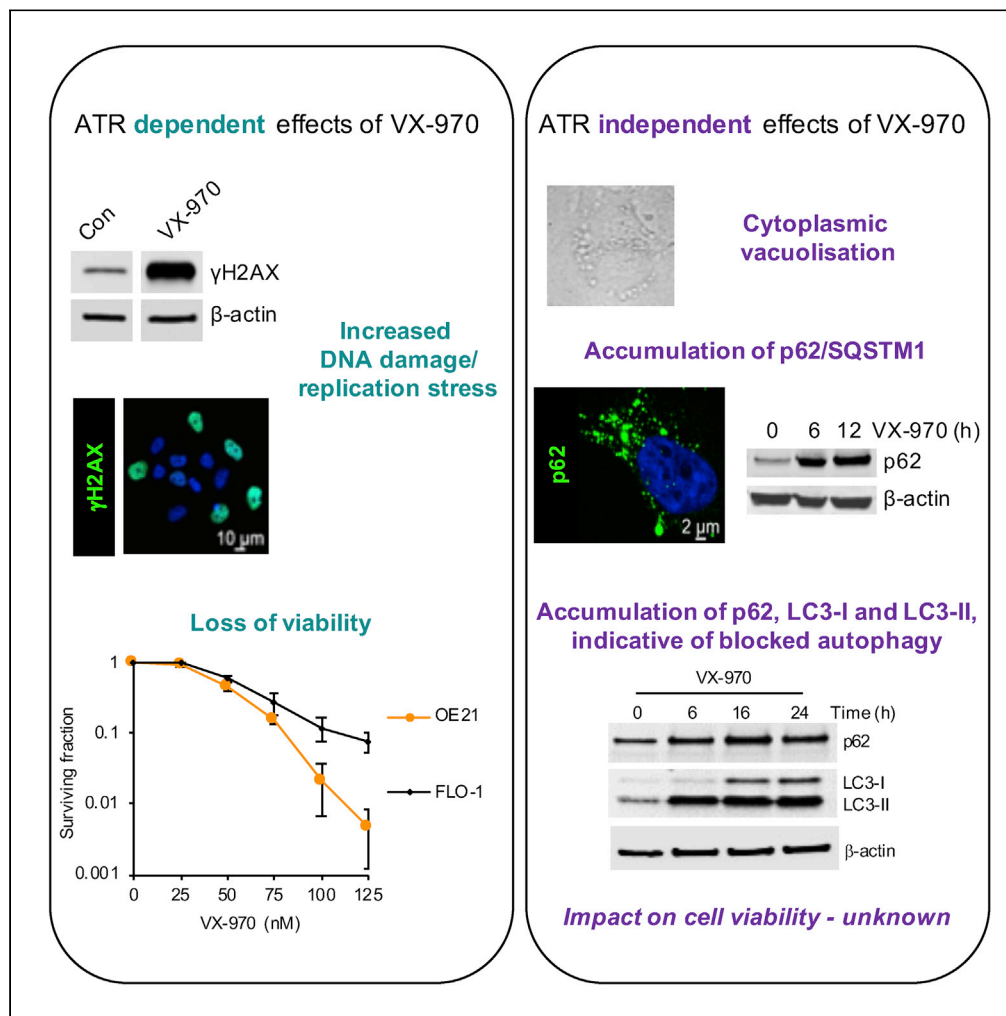


Article

# Pharmacological Inhibition of ATR Can Block Autophagy through an ATR-Independent Mechanism



Elizabeth Bowler,  
Anna Skwarska,  
Joseph D.  
Wilson, ...,  
Katarzyna B.  
Leszczynska,  
Stuart J. Conway,  
Ester M.  
Hammond

ester.hammond@oncology.ox.ac.uk

**HIGHLIGHTS**  
Inhibition of ATR using VX-970 leads to an accumulation of p62

VX-970-mediated accumulation of p62 occurs independently of ATR

VX-970-mediated accumulation of p62 is consistent with blocked autophagy



## Article

Pharmacological Inhibition  
of ATR Can Block Autophagy  
through an ATR-Independent Mechanism

Elizabeth Bowler,<sup>1</sup> Anna Skwarska,<sup>1</sup> Joseph D. Wilson,<sup>1</sup> Shaliny Ramachandran,<sup>1</sup> Hannah Bolland,<sup>1</sup>  
Alistair Easton,<sup>3</sup> Christian Ostheimer,<sup>1</sup> Ming-Shih Hwang,<sup>1</sup> Katarzyna B. Leszczynska,<sup>1,2</sup> Stuart J. Conway,<sup>4</sup>  
and Ester M. Hammond<sup>1,5,\*</sup>

## SUMMARY

**Inhibition of the ATR kinase has emerged as a therapeutically attractive means to target cancer since the development of potent inhibitors, which are now in clinical testing. We investigated a potential link between ATR inhibition and the autophagy process in esophageal cancer cells using four ATR inhibitors including two in clinical testing. The response to pharmacological ATR inhibitors was compared with genetic systems to investigate the ATR dependence of the effects observed. The ATR inhibitor, VX-970, was found to lead to an accumulation of p62 and LC3-II indicative of a blocked autophagy. This increase in p62 occurred post-transcriptionally and in all the cell lines tested. However, our data indicate that the accumulation of p62 occurred in an ATR-independent manner and was instead an off-target response to the ATR inhibitor. This study has important implications for the clinical response to pharmacological ATR inhibition, which in some cases includes the blockage of autophagy.**

## INTRODUCTION

Ataxia telangiectasia and Rad3-related (ATR) is an essential kinase that plays a pivotal role in the cellular response to replication stress and DNA damage (Saldivar et al., 2017). A number of small molecules have now been described that demonstrate potent specificity for the inhibition of the ATR kinase (Charrier et al., 2011; Foote et al., 2018; Wengner et al., 2019). The availability of ATR inhibitors has led to a number of preclinical studies in a variety of disease models and subsequent clinical testing (Leszczynska et al., 2016; Dillon et al., 2019; Vendetti et al., 2018; Pires et al., 2012). Many downstream targets of ATR have been described, including the checkpoint kinase Chk1, some of which are also potential biomarkers.

In addition to decreased phosphorylation of characterized downstream targets, ATR inhibitors have been demonstrated to have a number of less obvious effects such as impacting the transcription of specific genes, including an increase in genes involved in senescence-associated secretory pathways (SASP) and endoplasmic reticulum (ER) stress. For example, ATR inhibition (using VE-821) was found to lead to increased p62 expression at both the mRNA and protein levels (Muralidharan et al., 2016). p62 is also known as sequestosome 1 (SQSTM1), which is reflective of its role as a ubiquitin-binding scaffold protein that targets proteins for selective autophagy (Zaffagnini et al., 2018). Autophagy is a highly conserved cytoprotective process that allows the recycling of cellular components in response to stress and is often dysregulated in cancer (Dikic and Elazar, 2018). The loss of p62 expression is a commonly used marker of autophagy and therefore an increase in p62 can be interpreted as a blockage in autophagy (Klionsky et al., 2016). However, the reported induction of p62 observed in response to the ATR inhibitor, VE-821, was not linked to a blockage in autophagy as another commonly used marker of autophagy, light chain 3 (LC3), appeared unaffected (Muralidharan et al., 2016). In a follow-on study focused on melanoma, inhibition of ATR was again demonstrated to lead to the induction of SASP/ER stress, which included an accumulation of p62 and the transcription factor C/EBP homologous protein (CHOP) (Muralidharan et al., 2017). The accumulation of p62 has also been implicated in compromising DNA repair, genomic integrity, and in accelerated aging (Eliopoulos et al., 2016; Hewitt et al., 2016; Kang et al., 2015; Kwon et al., 2012). A recent report demonstrated that accumulation of p62 hindered recruitment of factors including BRCA1, Rad51, and RAP80 to

<sup>1</sup>Oxford Institute for Radiation Oncology, Department of Oncology, The University of Oxford, Oxford OX3 7DQ, UK

<sup>2</sup>Laboratory of Molecular Neurobiology, Neurobiology Center, Nencki Institute of Experimental Biology, Polish Academy of Sciences, Warsaw, Poland

<sup>3</sup>Translational Histopathology Lab, Oxford Cancer Centre, Oxford OX3 7DQ, UK

<sup>4</sup>Department of Chemistry, Chemistry Research Laboratory, University of Oxford, Mansfield Road, Oxford OX1 3TA, UK

<sup>5</sup>Lead Contact

\*Correspondence: [ester.hammond@oncology.ox.ac.uk](mailto:ester.hammond@oncology.ox.ac.uk)  
<https://doi.org/10.1016/j.isci.2020.101668>



double-strand breaks leading to a decreased ability to repair damaged DNA (Wang et al., 2016). p62 also plays a role in both the DNA- and cGAMP-stimulated degradation of STING, which acts as a negative regulator of interferon signaling (Prabakaran et al., 2018). Interestingly, oxidation of p62 has recently been reported and described as a redox-sensitive mechanism linking oxidative stress and autophagy (Carroll et al., 2018; Otten et al., 2018).

ATR inhibitors (AZD6738, VX-970/M6620, and BAY-1895344) are all currently being tested in a range of clinical trials (ClinicalTrials.gov). These include testing of VX-970 in a phase I dose escalation safety study in combination with chemoradiotherapy in esophageal and other solid cancers (EudraCT Number: 2015-003965-27). In this study, we set out to determine whether inhibition of ATR led to an accumulation of p62 in esophageal cell lines and to investigate the relevant mechanism and biological consequence.

## RESULTS

### VX-970 Treatment Leads to p62 Accumulation

Esophageal cancer cells are sensitive to ATR inhibition although the extent of the response varies (Figure S1A) (Leszczynska et al., 2016). We investigated the expression of p62 protein in response to VX-970 treatment in four esophageal cell lines, including both squamous and adenocarcinoma cell lines. In each case a significant increase in p62 was observed after VX-970 treatment (Figure 1A). The accumulation of p62 in response to VX-970 was not restricted to esophageal cell lines and was also observed in a lung adenocarcinoma cell line, A549 (Figure S1B). The accumulation of p62 in response to VX-970 was found to be dose dependent and was evident from 0.1  $\mu$ M (Figure S1C). Furthermore, we observed accumulation of p62 in response to VX-970 in three non-cancer cell lines, although this was less pronounced compared with the cancer cell lines (Figure 1B). To determine the cellular localization of p62 in VX-970 treated cells, we carried out both immunofluorescence analysis and cell fractionation. By microscopy, we saw significant accumulation of p62 predominantly in the cytoplasm of VX-970-treated OE21 cells with over 70% of the cells displaying increased p62 aggregates (Figures 1C and S1D). As a positive control for ATR inhibition, we also visualized  $\gamma$ H2AX and found that 50% of the cells were positive for pan-nuclear  $\gamma$ H2AX. Interestingly, cellular fractionation confirmed that both the cytoplasmic and nuclear expression of p62 increased (Figure 1D). To determine if p62 accumulation in these esophageal cell lines occurred via the same mechanism as previously reported, OE21 cells were treated with VX-970 in the absence of any other exogenous stress and qPCR carried out for the well-characterized target of ER stress; CHOP, as well as p62 (Muralidharan et al., 2016, 2017). Surprisingly and in contrast to the previous reports, neither the level of p62 nor CHOP mRNA was significantly altered in response to exposure to VX-970 (Figure 1E). To verify that CHOP is responsive to ER stress inducers, cells were also treated with thapsigargin or tunicamycin and a significant increase in CHOP was confirmed (Figure S1E). Together, these data demonstrate a significant accumulation of p62 protein in response to VX-970, which does not depend on increased mRNA levels of CHOP. Finally, we carried out immunohistochemistry on samples from a previous study (Leszczynska et al., 2016) to determine if p62 accumulated in OE-21 cells grown as xenograft tumors after treatment with VX-970. These data, although preliminary and limited by sample number ( $n = 3$ ), suggest that p62 expression is higher in VX-970-treated tumors compared with untreated (Figure S1F).

### VX-970 Leads to p62 Accumulation in an ATR-Independent Manner

Next, we sought to verify that the accumulation of p62 in response to VX-970 was the result of ATR inhibition. To achieve this, OE21 cells were exposed to alternative ATR inhibitors (VE-821, AZD6738, or BAY-1895344) and p62 levels were determined. Like VX-970 and as previously reported for other cancer types, exposure to the structurally related VE-821 led to an accumulation of p62 (Figure 2A). However, in contrast to treatment with VX-970 and VE-821, we saw no accumulation of p62 in cells treated with various concentrations of either AZD6738 or BAY-1895344 (Figures 2B and 2C), which are structurally distinct to VE-821 and VX-970. As expected, in response to all the ATR inhibitors  $\gamma$ H2AX increased, indicative of ATR inhibition (Figures 2B–2D and S2A). To rule out the possibility that the kinetics of p62 accumulation in response to AZD6738 or BAY-1895344 differed to those observed for VX-970, a time course was carried out. No accumulation of p62 was observed in response to AZD6738 or BAY-1895344 over a 24-h period (Figures S2B and S2C). These data suggest that the p62 accumulation in response to VX-970/VE-821 occurs independently of ATR inhibition. This was supported by the finding that inhibition of Chk1, a key downstream target of ATR, did not lead to accumulation of p62 (Figure S2D). To further test this hypothesis, we analyzed the levels of p62 in ATR heterozygous HCT116 cells, which express significantly less ATR protein than the matched controls. The baseline level of p62 in these cells was similar despite the difference in ATR, and in both cases,

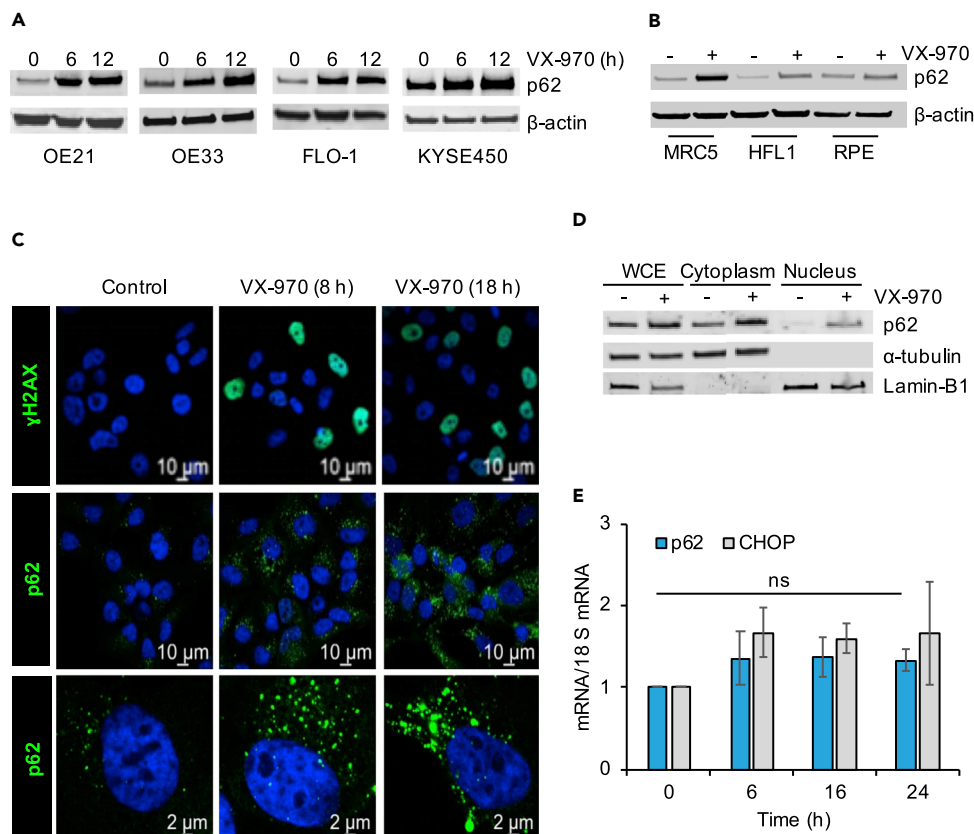


**Figure 1. VX-970 Treatment Leads to an Accumulation of p62**

(A) The esophageal cell lines indicated were treated with VX-970 (1  $\mu$ M) for the times shown. Western blotting was carried out for the detection of p62 expression.  $\beta$ -Actin was used as a loading control. OE21 (n = 3), OE33 (n = 2), FLO-1 (n = 2), KYSE (n = 1).

(B) MRC5, HFL1, and RPE cells were exposed to 1  $\mu$ M VX-970 for 14 h followed by western blotting as indicated.  $\beta$ -Actin was used as a loading control. MRC-5 (n = 2), HFL1/RPE (n = 1).

(C) OE21 cells were exposed to 1  $\mu$ M VX-970 for 8 and 18 h followed by staining for p62 (green) or  $\gamma$ H2AX (green). DAPI (blue) was used to visualize the nucleus (n = 2).

(D) OE21 cells were exposed to VX-970 (1  $\mu$ M) for 18 h and subjected to cellular fractionation to produce cytoplasmic and nuclear fractions. Whole-cell extracts (WCE) were included.  $\alpha$ -Tubulin and Lamin-B1 were used as cytoplasmic and nuclear controls, respectively (n = 3).

(E) OE21 cells were exposed to VX-970 (1  $\mu$ M) for the indicated times. qPCR was carried out to determine mRNA levels for p62 and CHOP, which were normalized to 18S mRNA. Data represent fold change in gene expression relative to DMSO control (0 h). Means  $\pm$  SD of three independent experiments are shown.

when VX-970 was added an increase in p62 was observed (Figure 2D). Next, we used cells from a patient with Seckel syndrome and a normal matched control. In this case the levels of p62 did differ between the two cell lines; however, it was the ATR proficient cell line that had the highest level of p62 (Figure 2E). Finally, we used siRNA to deplete ATR and determined the levels of p62. The siRNA treatment led to an almost complete loss of detectable ATR protein, but this had no impact on the levels of p62 (Figure 2F). Together, these data demonstrate that, although VE-821 and VX-970 led to an accumulation of p62, this is not due to inhibition of ATR. Kinase inhibitors are highly likely to inhibit related kinases to some extent and in the case of ATR inhibitors these are most likely ATM and DNA-pk. Although less significant, weak inhibition of mTOR has also been reported for some ATR inhibitors (Figure S3A). Inhibition of mTOR is predicted to lead to increased autophagy and reduced p62 and so is unlikely to explain the mechanism of p62 induction observed in response to VE-821 and VX-970 (Kakiuchi et al., 2019; Villar et al., 2017). The structures of the four ATR inhibitors we have investigated are shown (Figure 3). We considered whether the chemical properties of the compounds, including the predicted  $pK_a$ , protonation states (at pH 7.4), and cLog D values of the inhibitors correlate with the ability to induce p62. Although we found no such

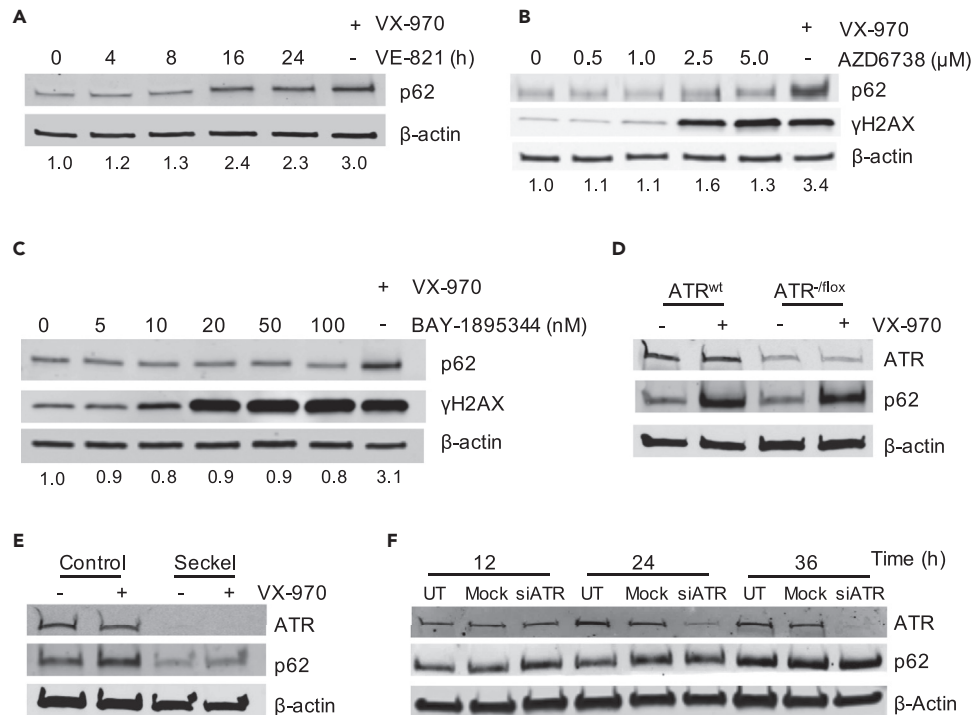


**Figure 2. Accumulation of p62 is Not Dependent on Inhibition of ATR**

(A) OE21 cells were exposed to 1  $\mu\text{M}$  VE-821 for the time points indicated ( $n = 3$ ).  
 (B) OE21 cells were exposed to the range of doses indicated of AZD6738 for 16 h ( $n = 3$ ).  
 (C) OE21 cells were treated with BAY-1895344 for a period of 16 h using the doses indicated ( $n = 2$ ). In (A)–(C) as a positive control, cells were treated with 1  $\mu\text{M}$  VX-970 for 16 h. Quantification of p62 expression normalized to  $\beta$ -actin (p62/ $\beta$ -actin) is shown as a fold change below the loading controls.  $\gamma\text{H2AX}$  was used as a marker for DNA damage.  
 (D) HCT116 ATR<sup>wt</sup> and HCT116 ATR<sup>-fllox</sup> cells were treated with 1  $\mu\text{M}$  VX-970 for 16 h followed by immunoblotting for the indicated proteins ( $n = 2$ ).  
 (E) Lymphoblastoid cells from a patient with Seckel syndrome and a normal matched control were exposed to VX-970 (1  $\mu\text{M}$ ) for 16 h followed by immunoblotting for the indicated proteins ( $n = 2$ ).  
 (F) OE21 cells were untreated (UT) or transfected with either ATR siRNA (siATR) or mock control (Mock). Cells were harvested at 12, 24, and 36 h post transfection and immunoblotting was carried out with the indicated antibodies ( $n = 3$ ).  $\beta$ -Actin was used as a loading control for all western blots.

relationship (Figures S3B–S3E), we note that VE-821 and VX-970 are structurally related and both incorporate the pyrazin-2-amine motif. AZD6738 and BAY-1895344 both possess an (*R*)-3-methylmorpholino group and are structurally distinct to VE-821 and VX-970.

### p62 Accumulates in a Redox-Independent Manner in Response to VX-970

Previous reports have determined that p62 levels increase in response to oxidative stress (Carroll et al., 2018). To test the hypothesis that VX-970-induced p62 might be the result of oxidative stress, we exposed OE21 cells to VX-970 in the presence of the ROS scavenger, *N*-acetyl-L-cysteine (NAC), and determined the impact on p62 accumulation. As expected, p62 and  $\gamma\text{H2AX}$  accumulated in response to VX-970; however, the addition of NAC abrogated the induction of p62 and significantly reduced  $\gamma\text{H2AX}$  (Figure 4A). This suggested that VX-970-mediated accumulation of p62 and DNA damage might be the result of increased ROS. The redox sensitivity of p62 was previously attributed to the formation of disulfide bonds between specific cysteine residues (105, 113) (Carroll et al., 2018). Using mouse embryonic fibroblasts (mefs) with these cysteines mutated to alanines, we asked if this mechanism was critical to the VX-970-dependent accumulation of p62. The matched mefs were exposed to VX-970 for up to 16 h followed by western blotting for p62. Preliminary results showed that VX-970 still led to p62 accumulation even in the mutant mefs, suggesting that p62 accumulation was independent of ROS (Figure S4A). To confirm whether VX-970 led to increased cellular ROS, we exposed OE21 cells to the ATR inhibitors and measured mitochondrial ROS using MitoSox

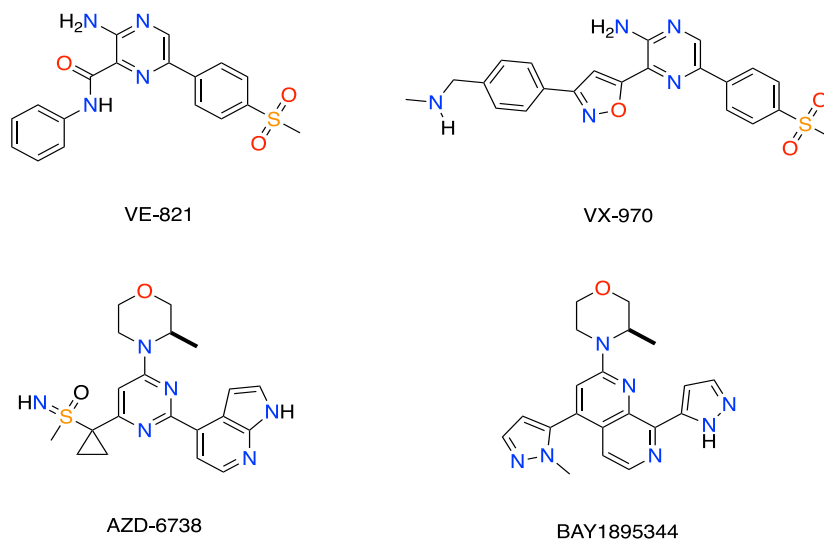


**Figure 3. The Chemical Structures of the ATR Inhibitors VE-821, VX-970, AZD6738, and BAY-1895344**

after a period of 6 h (Figures 4B and S4B–S4D). None of the four ATR inhibitors tested (VX-970, VE-821, AZD6738, or BAY-1895344) significantly induced ROS during this time frame. This finding was supported with a subsequent DCFDA ROS assay, which was undertaken in order to assess total cellular ROS levels, and again showed that the ATR inhibitors did not induce ROS in the time frame in which p62 accumulates (Figure 4C). Notably, longer exposure to the ATR inhibitors, including those that do not lead to p62 accumulation, resulted in the accumulation of mitochondrial ROS (Figures S5A–S5C). As expected, treatment with H<sub>2</sub>O<sub>2</sub> led to a significant increase in ROS, and therefore, we asked if p62 accumulated in these conditions. OE21 cells were exposed to H<sub>2</sub>O<sub>2</sub> but did not accumulate p62 (Figure 4D). Together, these data indicate that p62 is accumulating in a redox-independent manner and suggests that VX-970 leads to blockage in autophagy and subsequent p62 accumulation. To begin investigating this, we treated OE21 cells with chloroquine (CQ), a known autophagy blocker. As expected, treatment with CQ also led to p62 accumulation and surprisingly this too was inhibited by NAC treatment (Figure 4E). This finding is unexplained, although we did verify that CQ did not lead to increased ROS levels and so the effect on p62 accumulation is likely ROS independent (Figures S5D and S5E) and more likely dependent on the known non-specific activities of NAC (Halasi et al., 2013; Sun, 2010).

### VX-970 Leads to a Blockage in Autophagy

Cells exposed to VX-970 rapidly underwent cytoplasmic vacuolization demonstrated by the presence of translucent vesicles (Figure 5A). Cytoplasmic vacuolization has recently been reported in response to VX-970 in metastatic osteosarcoma cells where it was linked to eventual cell death but not autophagy (Li et al., 2020). However, we further investigated the hypothesis that VX-970 may block autophagy. During autophagy, LC3-I is lipidated to form LC3-II, which is required for forming fully functional autophagosomes. Therefore, LC3 is commonly used as a marker for autophagy (Klionsky et al., 2016). OE21 cells were exposed to VX-970, and the levels of LC3 were determined to investigate changes in baseline autophagy rates. As shown previously, the levels of p62 increased with time and both LC3-I and II accumulated, suggesting that autophagy was indeed blocked (Figure 5B). No changes in LC3 were observed after exposure to VE-821, AZD6738, or BAY-1895344 (Figures S6A–S6C). These data demonstrate that, although both VX-970 and VE-821 lead to an accumulation of p62, only VX-970 also impacts LC3. Next, OE21 cells were exposed to VX-970 in hypoxic conditions of <0.1% oxygen, which has been shown to induce autophagy (Rzymiski et al., 2010; Skwarska et al., 2017). As expected, exposure to hypoxia led to increased LC3-II and a decrease in p62. However, in the presence of VX-970 in hypoxia, the expression of LC3-II was further increased and p62 accumulated (Figure S6D). Again, this was not restricted to OE21 cells and was also observed in HCT116 and RKO cells (Figures S6E and S6F). This again suggests that autophagy flux is blocked by VX-970. Given that increased levels of LC3-II may indicate either increased formation of autophagosomes or blockage of autophagosome degradation, we next determined the effect of VX-970 on the autophagic

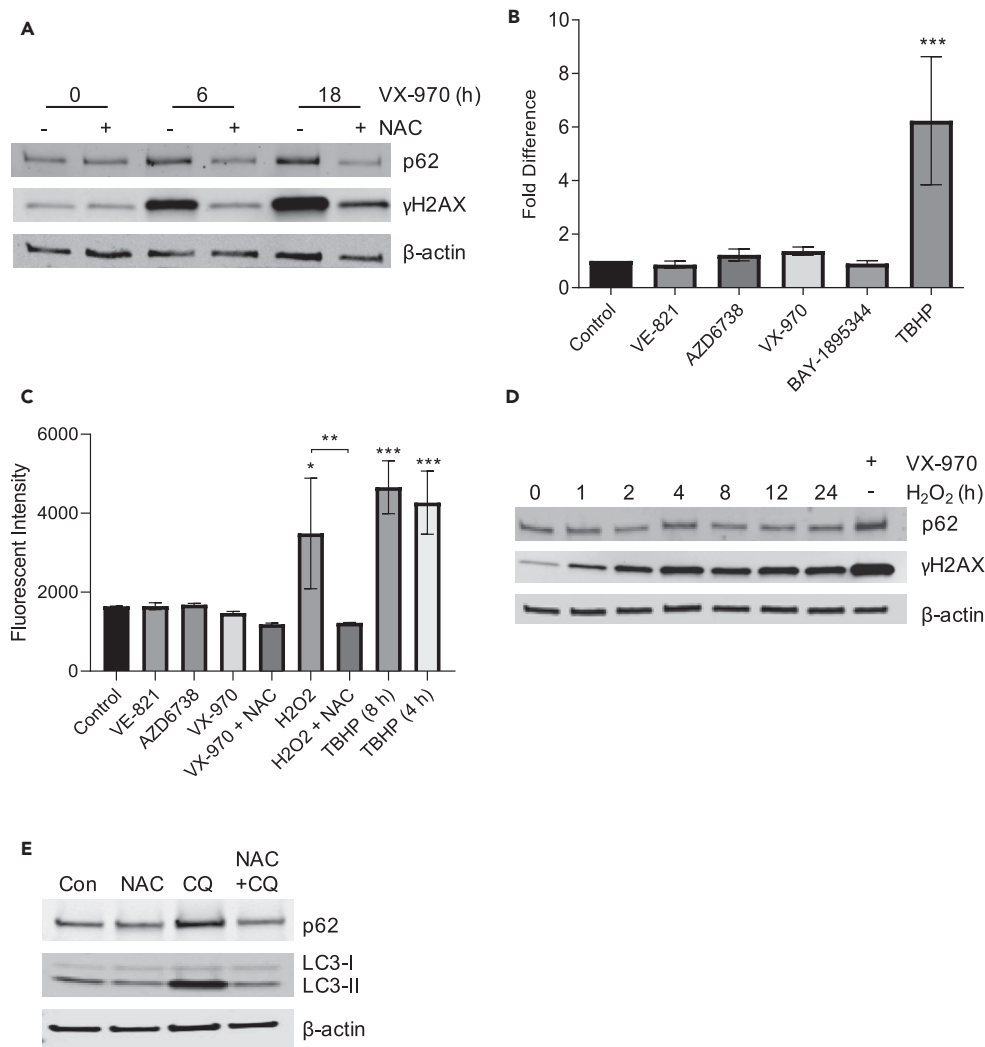


**Figure 4. ROS Dependence of p62 Accumulation**

(A) OE21 cells were treated with either VX-970 (1  $\mu$ M) alone or co-treated with NAC (20 mM) at the time points indicated. Western blotting was carried out using the antibodies indicated.  $\gamma$ H2AX was used to detect double-stranded breaks and  $\beta$ -actin was used as a loading control (n = 3).

(B) OE21 cells were treated with ATR inhibitors for 6 h as follows: VX-970 (1  $\mu$ M), VE-821 (1  $\mu$ M), AZD6738 (1  $\mu$ M), or BAY-1895344 (20 nM). Cells were stained with MitoSox (5  $\mu$ M) and assayed by flow cytometry. Tert-butyl hydroperoxide (TBHP) (150 mM) was used as positive control for ROS generation (p < 0.001 = \*\*\*) (n = 3).

(C) OE21 cells were treated with ATR inhibitors, VE-821 (1  $\mu$ M), AZD6738 (1  $\mu$ M) or VX-970 (1  $\mu$ M), for 8 h and ROS production was detected using the DCFDA ROS assay. H<sub>2</sub>O<sub>2</sub> (100  $\mu$ M) and TBHP (150 mM) were used as positive controls for ROS generation (\*p < 0.05; \*\*p < 0.01; \*\*\*p < 0.001) (n = 3).

(D) OE21 cells were treated with H<sub>2</sub>O<sub>2</sub> (1 mM) at varying time points indicated and p62 protein expression was determined. VX-970 (1  $\mu$ M, 18 h) was used as a positive control (n = 2).  $\gamma$ H2AX was used as a control for ATR inhibition and  $\beta$ -actin was used as a loading control.

(E) OE21 cells were exposed to chloroquine (CQ, 30  $\mu$ M) and/or NAC (20 mM) for 6 h. The levels of p62, LC3, and  $\beta$ -actin are shown (n = 2).

flux in the presence of autophagy inhibitors. Autophagy is a multistep process, and a number of autophagy modulators are in common use that block autophagy at different stages, such as 3-methyladenine (3-MA), which blocks the early stage by suppressing the formation of autophagosomes; CQ and bafilomycin A<sub>1</sub> (BafA1), which both block late stage autophagy through preventing fusion of the autophagosomes and lysosomes (Klionsky et al., 2016). If VX-970 alone increases the level of LC3-II, but there is no further increase

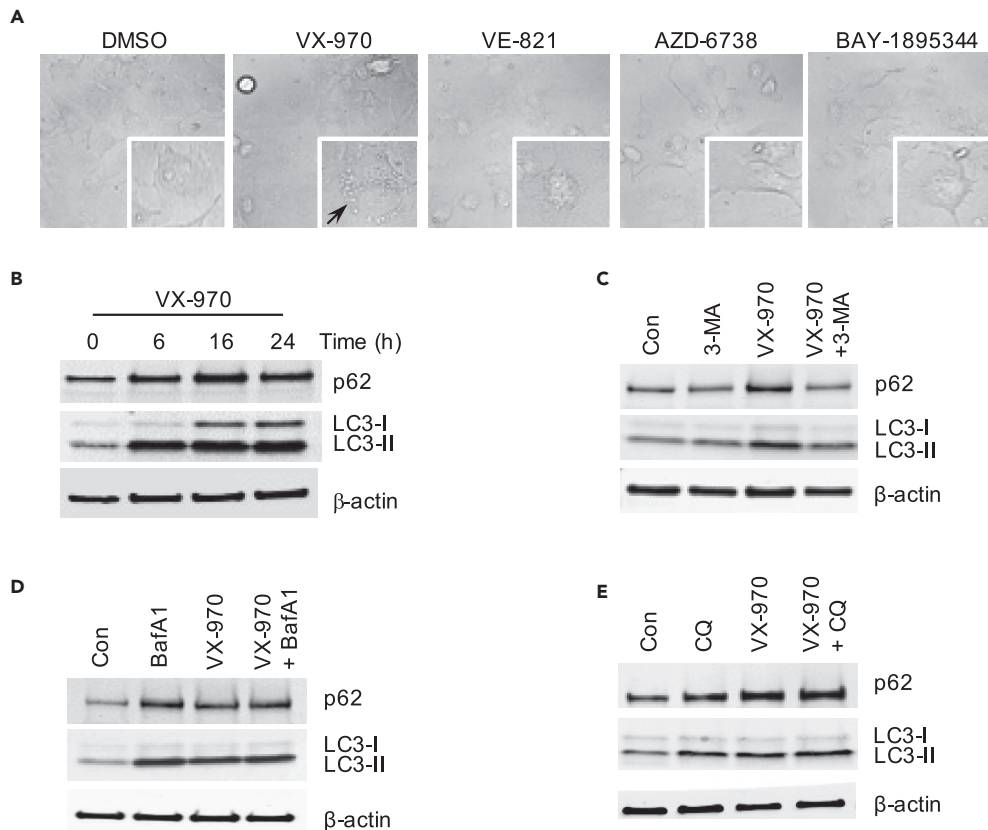


**Figure 5. VX-970 Treatment Leads to a Late-Stage Blockage in Autophagy**

(A) OE21 cells were treated with VX-970 (1  $\mu$ M), VE-821 (1  $\mu$ M), AZD-6738 (1  $\mu$ M), or BAY-1895344 (20 nM) for 8 h. Light microscopy demonstrates the presence of translucent vesicle (black arrow) in the live cells (n = 3). Images were taken using 20x objective.

(B) OE21 cells were exposed to VX-970 (1  $\mu$ M) for the times indicated followed by western blotting. The levels of p62, LC3, and  $\beta$ -actin are shown (n = 3).

(C) OE21 cells were exposed to 3-methyladenine (3-MA, 10 mM), VX-970 (1  $\mu$ M), or 3-MA + VX-970 for 6 h followed by western blotting. The levels of p62, LC3, and  $\beta$ -actin are shown (n = 3).

(D) OE21 cells were treated with bafilomycin A1 (BafA1, 100 nM), VX-970 (1  $\mu$ M), or BafA1 + VX-970 (1  $\mu$ M) for 6 h followed by western blotting. The levels of p62, LC3, and  $\beta$ -actin are shown (n = 3).

(E) OE21 cells were treated with VX-970 (1  $\mu$ M), CQ (100  $\mu$ M), or VX-970 + CQ for 6 h. CQ was added for 1 h before the end of VX-970 treatment. Western blotting was then carried out for p62, LC3, and  $\beta$ -actin (n = 2).

in the presence of the autophagy inhibitors, then it is likely that autophagy flux is inhibited by VX-970 and autophagosomes do not undergo autophagic degradation. Co-treatment of OE21 cells with 3-MA and VX-970 abrogated the p62 accumulation observed with VX-970 treatment alone (Figure 5C). These data indicate that blocking autophagy at an early stage prevented the accumulation of p62 suggesting that the VX-970-mediated effect on autophagy occurred at a later stage. Treatment with either BafA1 or CQ alone led to the expected increase in p62 confirming that these agents block autophagy in OE21 cells. However, when BafA1 or CQ were used in combination with VX-970 no further increase in p62 was observed (Figures 5D and 5E). Together, these data indicate that, like BafA1 and CQ, VX-970 blocks late-stage autophagy by inhibiting autophagy flux.

## DISCUSSION

This study has shown that induction of p62 protein by the ATR inhibitor, VX-970, occurs in an ATR-independent manner. This conclusion is based on evidence that an increase in p62 is attributed to only VX-970 and its precursor VE-821, whereas ATR inhibitors AZD6738 and BAY-1895344 have no effect on p62 levels.

Furthermore, p62 expression was unaffected or decreased in ATR-deficient cell lines when compared with matched controls, and siRNA knockdown of ATR had no effect on p62 levels. It is possible that both VE-821 and VX-970 have the same off-target effect mediated through their shared structural features, whereas AZD6738 and BAY-1895344 do not share these features and hence do not evoke the same biological effects. Future work is required to conclusively determine whether these findings translate to an *in vivo* setting. However, we present preliminary data in a limited dataset that indicates that VX-970-mediated accumulation of p62 is evident *in vivo*, suggesting that this could potentially be an informative biomarker in patients treated with VX-970.

A previous report linked p62 accumulation to oxidative stress; however, in our study we saw no evidence of increased ROS in response to VX-970 (Carroll et al., 2018). Somewhat confusingly, p62 accumulation upon VX-970 treatment was rescued by NAC, a ROS scavenger. NAC has been shown to have alternative functions in addition to a role as a ROS scavenger (Halasi et al., 2013; Sun, 2010). Therefore, it is probable that the abrogation of p62 induction by NAC is through another means and not due to its ROS scavenging function. Notably, p62 accumulation was also prevented by NAC in CQ-treated cells suggesting this is a general off-target effect. We have not pursued the use of alternative ROS scavengers instead of NAC as we have demonstrated that VX-970 does not increase ROS in the time frame in which p62 accumulates.

Our findings agree with previous studies, which describe an induction of p62 in response to ATR inhibition using VE-821 (Muralidharan et al., 2016, 2017). In contrast to these reports, we have not been able to link inhibition of ATR to an increase in ER stress as we saw no increase in *CHOP* expression; it is possible that this difference reflects a cell type-specific response. However, in agreement with the previous reports, we also concluded that, despite the accumulation of p62 in response to VE-821, there was no significant blockage in autophagy, as determined by LC3. Notably, the p62 accumulation after VE-821 treatment was not as robust as after VX-970, leading us to conclude that, if the off-target effect of VX-970 and VE-821 is the same, it is less potent with VE-821.

Based on the appearance of VX-970-treated cells, it seems that p62 is forming large aggregates or possibly p62 bodies that are either not targeted to the lysosome or are not being degraded (You et al., 2019). The consequence of increased p62 and/or blocked autophagy are difficult to predict and will undoubtedly be context dependent. However, autophagy is reported to be overactive in cancers and thought to play a role in tumor cell survival (Kimmelman and White, 2017) and an accumulation of p62 has been linked to a reduction in the repair of double-stranded DNA breaks (Wang et al., 2016). Therefore, it is possible that the additional property of inhibiting autophagy may increase the efficacy of VX-970 in clinical studies. Most importantly, this study highlights that caution is warranted when using pharmacological inhibitors as significant off-target effects can occur.

### Limitations of the Study

Our data using specific inhibitors to block different stages of autophagy suggest that VX-970 inhibits the later stages of autophagy. However, further assays including genetically blocking autophagosome initiation and using a mRFP-GFP-LC3 tandem fluorescent probe to study autophagic flux would be required to fully investigate the nature of the VX-970-mediated autophagy block (Yoshii and Mizushima, 2017; Klionsky et al., 2016). Further investigation is required to address important questions including how the accumulation of p62 and blockage of autophagy influence cell fate.

### Resource Availability

#### Lead Contact

Further information and requests for resources and reagents should be directed to and will be fulfilled by the Lead Contact, Ester Hammond ([ester.hammond@oncology.ox.ac.uk](mailto:ester.hammond@oncology.ox.ac.uk)).

#### Materials Availability

This study did not generate new unique reagents.

#### Data and Code Availability

This study did not generate/analyze datasets/code.

## METHODS

All methods can be found in the accompanying [Transparent Methods supplemental file](#).

## SUPPLEMENTAL INFORMATION

Supplemental Information can be found online at <https://doi.org/10.1016/j.isci.2020.101668>.

## ACKNOWLEDGMENTS

Thank you to Prof Andrew Thorburn (University of Colorado) for his advice and Prof Viktor Korolchuk (University of Newcastle) for the p62 mef cells lines. S.R./M.-S.H./K.B.L. were supported by a CRUK grant C5255/A23755 (awarded to E.M.H.). A.S. was supported by the MRC, MR/N009460/1 (awarded to S.J.C. and E.M.H.). H.B. was supported by an EPSRC grant EP/S019901/1 (awarded to S.J.C. and E.M.H.).

## AUTHOR CONTRIBUTIONS

Experiments were carried out by E.B., A.S., S.R., J.D.W., C.O., A.E., H.B., M.-S.H., K.B.L. The manuscript was written by E.B., S.J.C., and E.M.H. with input from all the authors.

## DECLARATION OF INTERESTS

The authors declare no competing interests.

Received: August 2, 2020

Revised: September 25, 2020

Accepted: October 7, 2020

Published: November 20, 2020

## REFERENCES

- Carroll, B., Otten, E.G., Manni, D., Stefanatos, R., Menzies, F.M., Smith, G.R., Jurk, D., Kenneth, N., Wilkinson, S., Passos, J.F., et al. (2018). Oxidation of SQSTM1/p62 mediates the link between redox state and protein homeostasis. *Nat. Commun.* **9**, 256.
- Charrier, J.D., Durrant, S.J., Golec, J.M., Kay, D.P., Knechtel, R.M., McCormick, S., Mortimore, M., O'donnell, M.E., Pinder, J.L., Reaper, P.M., et al. (2011). Discovery of potent and selective inhibitors of ataxia telangiectasia mutated and Rad3 related (ATR) protein kinase as potential anticancer agents. *J. Med. Chem.* **54**, 2320–2330.
- Dikic, I., and Elazar, Z. (2018). Mechanism and medical implications of mammalian autophagy. *Nat. Rev. Mol. Cell Biol.* **19**, 349–364.
- Dillon, M.T., Bergerhoff, K.F., Pedersen, M., Whittock, H., Crespo-Rodriguez, E., Patin, E.C., Pearson, A., Smith, H.G., Paget, J.T.E., Patel, R.R., et al. (2019). ATR inhibition potentiates the radiation-induced inflammatory tumor microenvironment. *Clin. Cancer Res.* **25**, 3392–3403.
- Eliopoulos, A.G., Havaki, S., and Gorgoulis, V.G. (2016). DNA damage response and autophagy: a meaningful partnership. *Front. Genet.* **7**, 204.
- Foote, K.M., Nissink, J.W.M., Mcguire, T., Turner, P., Guichard, S., Yates, J.W.T., Lau, A., Blades, K., Heathcote, D., Odedra, R., et al. (2018). Discovery and characterization of AZD6738, a potent inhibitor of ataxia telangiectasia mutated and Rad3 related (ATR) kinase with application as an anticancer agent. *J. Med. Chem.* **61**, 9889–9907.
- Halasi, M., Wang, M., Chavan, T.S., Gaponenko, V., Hay, N., and Gartel, A.L. (2013). ROS inhibitor N-acetyl-L-cysteine antagonizes the activity of proteasome inhibitors. *Biochem. J.* **454**, 201–208.
- Hewitt, G., Carroll, B., Sarallah, R., Correia-Melo, C., Ogrodnik, M., Nelson, G., Otten, E.G., Manni, D., Antrobus, R., Morgan, B.A., et al. (2016). SQSTM1/p62 mediates crosstalk between autophagy and the UPS in DNA repair. *Autophagy* **12**, 1917–1930.
- Kakiuchi, Y., Yurube, T., Kakutani, K., Takada, T., Ito, M., Takeoka, Y., Kanda, Y., Miyazaki, S., Kuroda, R., and Nishida, K. (2019). Pharmacological inhibition of mTORC1 but not mTORC2 protects against human disc cellular apoptosis, senescence, and extracellular matrix catabolism through Akt and autophagy induction. *Osteoarthritis Cartilage* **27**, 965–976.
- Kang, C., Xu, Q., Martin, T.D., Li, M.Z., Demaria, M., Aron, L., Lu, T., Yankner, B.A., Campisi, J., and Elledge, S.J. (2015). The DNA damage response induces inflammation and senescence by inhibiting autophagy of GATA4. *Science* **349**, aaa5612.
- Kimmelman, A.C., and White, E. (2017). Autophagy and tumor metabolism. *Cell Metab.* **25**, 1037–1043.
- Klionsky, D.J., Abdelmohsen, K., Abe, A., Abedin, M.J., Abeliovich, H., Acevedo Arozana, A., Adachi, H., Adams, C.M., Adams, P.D., Adeli, K., et al. (2016). Guidelines for the use and interpretation of assays for monitoring autophagy (3rd edition). *Autophagy* **12**, 1–222.
- Kwon, J., Han, E., Bui, C.B., Shin, W., Lee, J., Lee, S., Choi, Y.B., Lee, A.H., Lee, K.H., Park, C., et al. (2012). Assurance of mitochondrial integrity and mammalian longevity by the p62-Keap1-Nrf2-Nqo1 cascade. *EMBO Rep.* **13**, 150–156.
- Leszczynska, K.B., Dobrynin, G., Leslie, R.E., Ient, J., Boumelha, A.J., Senra, J.M., Hawkins, M.A., Maughan, T., Mukherjee, S., and Hammond, E.M. (2016). Preclinical testing of an Atr inhibitor demonstrates improved response to standard therapies for esophageal cancer. *Radiother. Oncol.* **121**, 232–238.
- Li, X., Dean, D.C., Cote, G.M., Zou, L., Hornicek, F.J., Yu, S., and Duan, Z. (2020). Inhibition of ATR-Chk1 signaling blocks DNA double-strand-break repair and induces cytoplasmic vacuolization in metastatic osteosarcoma. *Ther. Adv. Med. Oncol.* **12**, 1758835920956900.
- Muralidharan, S.V., Bhadury, J., Nilsson, L.M., Green, L.C., Mclure, K.G., and Nilsson, J.A. (2016). BET bromodomain inhibitors synergize with ATR inhibitors to induce DNA damage, apoptosis, senescence-associated secretory pathway and ER stress in Myc-induced lymphoma cells. *Oncogene* **35**, 4689–4697.
- Muralidharan, S.V., Einarsdottir, B.O., Bhadury, J., Lindberg, M.F., Wu, J., Campeau, E., Bagge, R.O., Stiermer, U., Ny, L., Nilsson, L.M., et al. (2017). BET bromodomain inhibitors synergize with ATR inhibitors in melanoma. *Cell Death Dis.* **8**, e2982.
- Otten, E.G., Stefanatos, R., Carroll, B., and Korolchuk, V.I. (2018). Oxidation of p62 as an evolutionary adaptation to promote autophagy in stress conditions. *Cell Stress* **2**, 91–93.
- Pires, I.M., Olcina, M.M., Anbalagan, S., Pollard, J.R., Reaper, P.M., Charlton, P.A., Mckenna, W.G., and Hammond, E.M. (2012). Targeting radiation-

resistant hypoxic tumour cells through ATR inhibition. *Br. J. Cancer* 107, 291–299.

Prabakaran, T., Bodda, C., Krapp, C., Zhang, B.C., Christensen, M.H., Sun, C., Reinert, L., Cai, Y., Jensen, S.B., Skouboe, M.K., et al. (2018). Attenuation of cGAS-STING signaling is mediated by a p62/SQSTM1-dependent autophagy pathway activated by TBK1. *EMBO J.* 37, e97858.

Rzymiski, T., Milani, M., Pike, L., Buffa, F., Mellor, H.R., Winchester, L., Pires, I., Hammond, E., Ragoussis, I., and Harris, A.L. (2010). Regulation of autophagy by ATF4 in response to severe hypoxia. *Oncogene* 29, 4424–4435.

Saldívar, J.C., Cortez, D., and Cimprich, K.A. (2017). The essential kinase ATR: ensuring faithful duplication of a challenging genome. *Nat. Rev. Mol. Cell Biol.* 18, 622–636.

Skwarska, A., Ramachandran, S., Dobrynin, G., Leszczynska, K.B., and Hammond, E.M. (2017). The imidazoacridinone C-1311 induces p53-dependent senescence or p53-independent

apoptosis and sensitizes cancer cells to radiation. *Oncotarget* 8, 31187–31198.

Sun, S.Y. (2010). N-acetylcysteine, reactive oxygen species and beyond. *Cancer Biol. Ther.* 9, 109–110.

Vendetti, F.P., Karukonda, P., Clump, D.A., Teo, T., Lalonde, R., Nugent, K., Ballew, M., Kiesel, B.F., Beumer, J.H., Sarkar, S.N., et al. (2018). ATR kinase inhibitor AZD6738 potentiates CD8+ T cell-dependent antitumor activity following radiation. *J. Clin. Invest.* 128, 3926–3940.

Villar, V.H., Nguyen, T.L., Delcroix, V., Teres, S., Bouche-careilh, M., Salin, B., Bodineau, C., Vacher, P., Priault, M., Soubeyran, P., et al. (2017). mTORC1 inhibition in cancer cells protects from glutaminolysis-mediated apoptosis during nutrient limitation. *Nat. Commun.* 8, 14124.

Wang, Y., Zhang, N., Zhang, L., Li, R., Fu, W., Ma, K., Li, X., Wang, L., Wang, J., Zhang, H., et al. (2016). Autophagy regulates chromatin ubiquitination in DNA damage response through elimination of SQSTM1/p62. *Mol. Cell* 63, 34–48.

Wengner, A.M., Siemeister, G., Lucking, U., Lefranc, J., Wortmann, L., Lienau, P., Bader, B., Bomer, U., Moosmayer, D., Eberspacher, U., et al. (2019). The novel ATR inhibitor BAY 1895344 is efficacious as monotherapy and combined with DNA damage-inducing or repair-compromising therapies in preclinical cancer models. *Mol. Cancer Ther.* 19, 26–38.

Yoshii, S.R., and Mizushima, N. (2017). Monitoring and measuring autophagy. *Int. J. Mol. Sci.* 18, 1865.

You, Z., Jiang, W.X., Qin, L.Y., Gong, Z., Wan, W., Li, J., Wang, Y., Zhang, H., Peng, C., Zhou, T., et al. (2019). Requirement for p62 acetylation in the aggregation of ubiquitylated proteins under nutrient stress. *Nat. Commun.* 10, 5792.

Zaffagnini, G., Savova, A., Danieli, A., Romanov, J., Tremel, S., Ebner, M., Peterbauer, T., Sztacho, M., Trapannone, R., Tarafder, A.K., et al. (2018). p62 filaments capture and present ubiquitinated cargos for autophagy. *EMBO J.* 37, e98308.

iScience, Volume 23

## **Supplemental Information**

### **Pharmacological Inhibition of ATR Can Block Autophagy through an ATR-Independent Mechanism**

**Elizabeth Bowler, Anna Skwarska, Joseph D. Wilson, Shaliny Ramachandran, Hannah Bolland, Alistair Easton, Christian Ostheimer, Ming-Shih Hwang, Katarzyna B. Leszczynska, Stuart J. Conway, and Ester M. Hammond**

## SI FIGURE LEGENDS

Figure S1. **VX-970 leads to an accumulation of p62, related to figure 1**

**A.** OE21, FLO-1 and KYSE450 oesophageal cancer cell lines were treated with the indicated concentrations of VX-970 and colony survival was assessed after 1-2 weeks. The graph shows mean  $\pm$  SEM of 3 biological repeats. **B.** A549 cells were exposed to VX-970 (1  $\mu$ M) for the times indicated followed by western blotting for p62 and  $\beta$ -actin as a loading control (n=2). **C.** OE21 cells were exposed to the range of doses of VX-970 indicated for 24 hours followed by western blotting for p62 and  $\beta$ -actin (n=2). **D.** OE21 cells were exposed to 1  $\mu$ M VX-970 for 8 and 18 hours followed by staining for p62 (green). DAPI (blue) was used to visualise the nucleus. **E.** OE21 cells were exposed to Tunicamycin (5  $\mu$ g/mL) or Thapsigargin (2  $\mu$ M) for 6 h. qPCR was then carried out for measurement of CHOP mRNA expression relative to 18S. Means  $\pm$  SD of 3 independent experiments are shown. **F.** OE21 cells were grown as xenograft tumours in mice treated with either vehicle (10% vitamin E d-alpha tocopherol polyethylene glycol 1000 succinate) or 60 mg/kg VX-970 orally as previously described (Leszczynska et al., 2016). Sections from the tumours were stained with p62. i: Secondary antibody alone control. ii-iv: Vehicle treated control mice. v-vii: VX-970-treated mice. Images represent individual mice (n=3).

Figure S2. **VX-970 dependent induction of p62 occurs independently of ATR, related to figure 2**

**A.** OE21 cells were treated with VE-821 (1  $\mu$ M) (n=1). **B.** OE21 cells were exposed to AZD6738 (1  $\mu$ M) or **C.** BAY-1895344 (20 nM) for the times indicated. VX-970 (1  $\mu$ M for 18 hours) was used as a positive control for p62 induction and the levels of  $\gamma$ H2AX are shown to demonstrate inhibition of ATR (n=2). **D.** OE21 cells were treated for 18 hours with VX-970 (1  $\mu$ M), VE-821 (1  $\mu$ M), AZD6738 (1  $\mu$ M) and the Chk1 inhibitor MK-8776 (1  $\mu$ M) (n>3 for ATR inhibitors, n=2 for Chk1 inhibitor). Western blotting was then carried out for the antibodies indicated.  $\beta$ -actin was used as a loading control for all western blots.

Figure S3. **Chemical properties of the four ATR inhibitors studied, related to figure 3**

**A.** IC<sub>50</sub> values for the ATR inhibitors are stated where available. Sources of the information are indicated below the table. The structures, predicted pK<sub>a</sub> values, predicted protonation states at pH 7.4, and cLog D values at pH 4.6 and pH 7.4 of the ATR inhibitors **B.** VE-821, **C.** VX-970, **D.** AZD-6738 and **E.** BAY1895344 are shown. Values were calculated using ACD/I-Lab v5.0.0.184.

Figure S4. **ROS dependence of p62 accumulation, related to figure 4**

**A.** Mefs with different status of p62 (p62<sup>-/-</sup>, p62<sup>+/+</sup>, p62<sup>-/-</sup> stably expressing FLAG-p62 and p62<sup>-/-</sup> stably expressing FLAG-C105,113Ap62) were treated with VX-970 (1  $\mu$ M) for the times indicated. Western blotting was then carried out for p62 expression.  $\beta$ -actin was used as a loading control and FLAG was used for the expression of FLAG tagged p62 (n=1). OE21 cells were treated with ATR inhibitors for 6 hours as follows; **B.** VE-821 (1  $\mu$ M), **C.** AZD6738 (1  $\mu$ M), **D.** BAY-1895344 (20 nM) and VX-970 (1  $\mu$ M) (shown in all). Cells were stained with MitoSox (5  $\mu$ M) and assayed by flow cytometry. Tert-Butyl hydroperoxide (TBHP) (150 mM) were used as positive control for ROS generation (p<0.001 = \*\*\*) (n=3). (B-D) Representative histograms for Figure 4B.

Figure S5. **Prolonged inhibition of ATR leads to increased ROS in OE21 cells, related to figure 4.**

OE21 cells were treated with **A.** VX-970 (1  $\mu$ M, 18 hours) **B.** VE-821 (1  $\mu$ M, 18 hours) and **C.** AZD6738 (1  $\mu$ M, 18 hours). NAC (20 mM, 18 hours) was used as a ROS scavenger and H<sub>2</sub>O<sub>2</sub> was used as a positive control. FACS analysis was then carried out using MitoSOX. Left-hand panels represent quantifications of FACS histograms represented in the right-hand panel. Results shown are mean  $\pm$  SD (n = 3). Significance: One-way ANOVA test, \*\*\*\* P < 0.0001. Histograms are representative of (n = 3). **D.** OE21 cells were treated for 6 hours with either VX-970 (1  $\mu$ M) or the autophagy inhibitor chloroquine (100  $\mu$ M). FACS

analysis was then carried out using MitoSOX. TBHP was used as a positive control for ROS induction. Results shown are mean  $\pm$  SEM (n = 3). Data analysis was conducted with a One-way ANOVA test, \*\*\*  $P < 0.001$ . This experiment was conducted at the same time as the results shown in Figure 4B and so the values for the control, VX-970 and TBHP are also displayed in Figure 4B. A representative FACS histogram is shown in E.

**Figure S6. VX-970 blocks hypoxia-induced autophagy, related to figure 5.**

OE21 cells were exposed to the ATR inhibitors indicated followed by western blotting. **A.** VE-821 (1  $\mu$ M), **B.** AZD6738 (1  $\mu$ M) and **C.** BAY-1895344 (20 nM). **D.** OE21, **E.** HCT116 and **F.** RKO cells were exposed to hypoxia (<0.1% O<sub>2</sub>) for the times indicated in the presence of VX-970 (1  $\mu$ M). Western blotting was carried out with the antibodies indicated. HIF-1 $\alpha$  was used as a positive control for hypoxia treatment, LC3-II was used as a marker for autophagy and  $\beta$ -actin was used as a loading control (n=1).

## Transparent Methods

### Cell lines and reagents

Oesophageal cell lines OE21 and OE33 squamous carcinoma cells (SCCs) and FLO-1 adenocarcinoma cells (ACA) were obtained from PHE culture collections (Salisbury, UK). A549 lung adenocarcinoma cells and colorectal cell lines; RKO and HCT116, were obtained from ATCC and cultured in DMEM supplemented with 10% FBS. The SCCs were cultured in RPMI supplemented with 10% FBS, while the ACAs were cultured in DMEM supplemented with 10% FBS. KYSE450 (DSMZ, Braunschweig, Germany) oesophageal SCCs were cultured in RPMI:HAM-F12 (1:1) and supplemented with 10% FBS. MRC5 foetal lung fibroblast-like and retinal pigment epithelium cells (RPE) were a gift from Dr. Geoff Higgins (University of Oxford, Oxford, UK) and were cultured in EMEM, supplemented with 10% FBS. HFL1 foetal lung fibroblasts (CCL-153; ATCC Teddington, Middlesex, UK) were cultured in F12K supplemented with 10% FBS. HCT116<sup>ATR-/flox</sup> cells (Bencokova et al., 2009) were cultured in DMEM supplemented with 15% FBS. Seckel cells and matched control were generously provided by Prof Grant Stewart (University of Birmingham, Birmingham, UK) and cultured in RPMI supplemented with 15% FBS. p62 wild-type (p62<sup>+/+</sup>), p62 knock-out (p62<sup>-/-</sup>), FLAG-p62 and FLAG-C105, C113A p62 mouse embryonic fibroblasts (mefs) (generously provided by Prof Viktor Korolchuk, Newcastle University, Newcastle, UK) were cultured in DMEM supplemented with 10% FBS and maintained in low levels of blasticidin (4  $\mu$ g/ml) until seeding for experimental purposes. ATR inhibitors used in this study were; VX-970 (also known as M6620) (MedChemExpress, New Jersey, USA), VE-821 (Tocris, Oxford, UK), AZD6738 (MedChemExpress, New Jersey, USA) and BAY-1895344 (S8666, Selleckchem, Munich, Germany). Cells exposed to hypoxia were put in a Bactron chamber (Sheldon Manufacturing INC, Oregon, USA) at <0.1% O<sub>2</sub>. Cells were harvested in hypoxic conditions using equilibrated solutions. For siRNA-mediated knockdown of ATR, OE21 cells were transfected with siRNA using DharmaFECT 1 (T-2001-03; Horizon Discovery, Cambridge, UK) following manufacturer's protocols. The ATR siRNA used was CAG GCA CTA ATT GTT CTT CAA.

### Cellular fractionation

Whole cell extract (WCE) plates were run alongside each of the cellular fractionation treated plates. After treatment with VX-970, all cells were washed in PBS. The extraction of WCE samples is outlined in the immunoblotting method. Buffer I (20 mM Tris pH 7.4, 2.5 mM MgCl<sub>2</sub> and 0.5% (w/w) NP40) was added to the fractionation plates and cells were scraped and centrifuged to separate the samples into nuclear (pellet) and cytoplasmic (supernatant) fractions. The pellet was washed in PBS before another round of centrifugation, and resuspended in Buffer II (20 mM PO<sub>4</sub> buffer pH 8.0, 0.5 M NaCl, 1 mM EDGA pH 8.0,

0.75% (w/w) Triton-X 100, 10% (w/w) glycerol, 5 mM MgCl<sub>2</sub>). Finally, 25 µg of protein was loaded for immunoblotting.

#### Immunoblotting

Immunoblotting was carried out as previously described using UTB lysis buffer (Dobrynin *et al.*, 2017). Primary antibodies used in this study were p62 (5114 and 88588; Cell Signaling, Leiden, The Netherlands),  $\beta$ -actin (sc-69879; Santa-Cruz Biotechnology, Dallas, Texas, USA), LC3 (2775s; Cell Signaling, Leiden, The Netherlands), LC3 (used only in Figure S6) (M115-3; MBL International Corporation, Massachusetts, USA), HIF-1 $\alpha$  (610958; Becton Dickinson Biosciences, San Jose, California, USA), ATR (sc-515173; Santa Cruz Biotechnology, Dallas, Texas, USA),  $\gamma$ H2AX (05-636; Millipore, Watford, Hertfordshire, UK), FLAG (F3165; Sigma Aldrich, Gillingham, Dorset, UK), lamin  $\beta$ 1 (PA5-19468; ThermoFisher Scientific, Loughborough, Leicestershire),  $\alpha$ -tubulin (sc-5286; Santa Cruz Biotechnology, Dallas, Texas, USA). Secondary antibodies used were IRDye 680RD goat anti-rabbit IgG (926-68071; LI-COR, Lincoln, Nebraska, USA), IR Dye 800CW goat anti-rabbit IgG (926-32211; LI-COR, Lincoln, Nebraska, USA), IR Dye 680RD goat anti-mouse IgG (926-68070; LI-COR, Lincoln, Nebraska, USA) and IR dye 800CW goat anti-mouse IgG (926-32210; LI-COR, Lincoln, Nebraska, USA). Western blots were visualised using an Odyssey infrared imaging system (LI-COR, software version 3.0). To quantify protein levels, we used ImageJ to determine optical density peak values for p62 bands and  $\beta$ -actin loading control, and then calculated p62 / loading control. All values were normalised to the 0 h value to give a fold change.

#### Immunofluorescence

OE21 cells were seeded on coverslips, treated and fixed with 4% PFA for 10 minutes, permeabilised with 1% Triton X-100 for 10 minutes and blocked with 2% BSA in 0.1% PBS-Tween-20. Primary antibodies mouse  $\gamma$ H2AX (05-636; Millipore, Watford Hertfordshire, UK) and mouse p62 (88588; Cell Signaling, Leiden, The Netherlands) were added onto separate coverslips overnight at 4°C followed by appropriate secondary antibodies for 1 hour at room temperature. Cells were mounted with ProLong Gold Antifade Mountant with DAPI (P36935; ThermoFisher, Lutterworth, Leicestershire, UK) and imaged using LSM780 confocal microscope (Carl Zeiss Microscopy Ltd, Cambourne, Cambridge, UK).

#### Immunohistochemistry

Xenografts were generated and treated with VX-970 as previously described (Leszczynska *et al.*, 2016). Paraffin-embedded tissue blocks from formalin fixed tumour samples were sectioned, dewaxed and rehydrated. Antigen retrieval was performed with 0.1 M citric acid buffer pH 6 at 110°C for 2 minutes. Endogenous peroxidase activity was blocked with 3% H<sub>2</sub>O<sub>2</sub> for 20 minutes at room temperature. Following blocking of non-specific binding with horse serum (s-2000; Vector Labs, Peterborough, Cambridgeshire, UK) for 1.5 hours and M.O.M reagent (MPX-2402; Vector Labs) for 45 minutes at room temperature, samples were incubated with p62 primary antibody (88588; Cell Signaling, Leiden, The Netherlands) for 1 hour at room temperature. Following a TBS wash, samples were incubated for secondary antibody from the Impress™ Kit (Vector Labs) for 30 minutes at room temperature. 3,3'-Diaminobenzidine (DAB) (H-2200; Vector Labs) was applied to the slide for 7 minutes, slides were counterstained with filtered haematoxylin (Sigma-Aldrich, Gillingham, Dorset, UK) solution for 3 minutes and mounted with Aquatex (1.08562; Sigma-Aldrich). Secondary only control staining was negative. Samples were scanned using the Vectra Polaris (AkoyaBio, California, USA) slide scanner. p62 staining was quantified by an independent blinded pathologist using the HALO® image analysis platform.

#### qPCR

qPCR was carried out as described previously (Dobrynin et al., 2017). Briefly, total RNA was extracted using TRI reagent (Sigma) according to the manufacturer's protocol and measured using a NanoDrop (Thermo Scientific). cDNA was synthesised using the Verso cDNA Enzyme kit (Life Technologies) and qPCR was carried out with SYBR mix using a Step One Plus Real-time PCR Detection System (Applied Biosystems). Primer sequences were as follows: p62 (F:GCTGCCCTATACCCACATCT; R:CGCCTTCATCCGAGAAAC), CHOP (F:GGAGCATCAGTCCCCCACTT; R:TGTGGGATTGAGGGTCACA), 18S (F:TAGAGGGACAAGTGGCGTTC; R:CGGACATCTAAGGGCATCAC). All mRNA expression levels were normalised to 18S mRNA. The quantitative PCR values were determined for each of the mRNAs levels using the comparative CT ( $\Delta\Delta CT$ ) method. Significance was determined using a one-way Anova with Dunnett's multiple comparison test.

#### ROS measurements

For Mitosox detection, cell pellets were resuspended in 5  $\mu$ M MitoSOX red mitochondrial superoxide indicator for live cell imaging (M36008; ThermoFisher Scientific, Lutterworth, Leicestershire) diluted in Hank's Buffered Salt Solution (HBSS) and incubated at 37°C for 10 minutes in the dark. Cells were once again pelleted and resuspended in HBSS before FACs analysis was performed using a BD FACSCalibur. Data was analysed using FlowJo software. The DCFDA cellular ROS detection assay kit (ab113851; Abcam, Cambridge, UK) was used as per the manufacturer's instructions for prolonged incubations. Briefly, cells were seeded onto 96-well plates in triplicate and treated with the compound of interest in fresh media. The treated media was replaced with 30  $\mu$ M DCFDA made up in 1 x buffer solution treated with the compound of interest 30 mins prior to the completion of the experiment. Plates were protected from light and incubated at 37°C for 30 minutes before measurement with a Polestar microplate reader at Ex/Em = 520 nm with 1000 gain and shaking. Data was analysed with GraphPad Prism 8 using an ordinary one-way ANOVA with multiple comparisons.

#### Colony survival

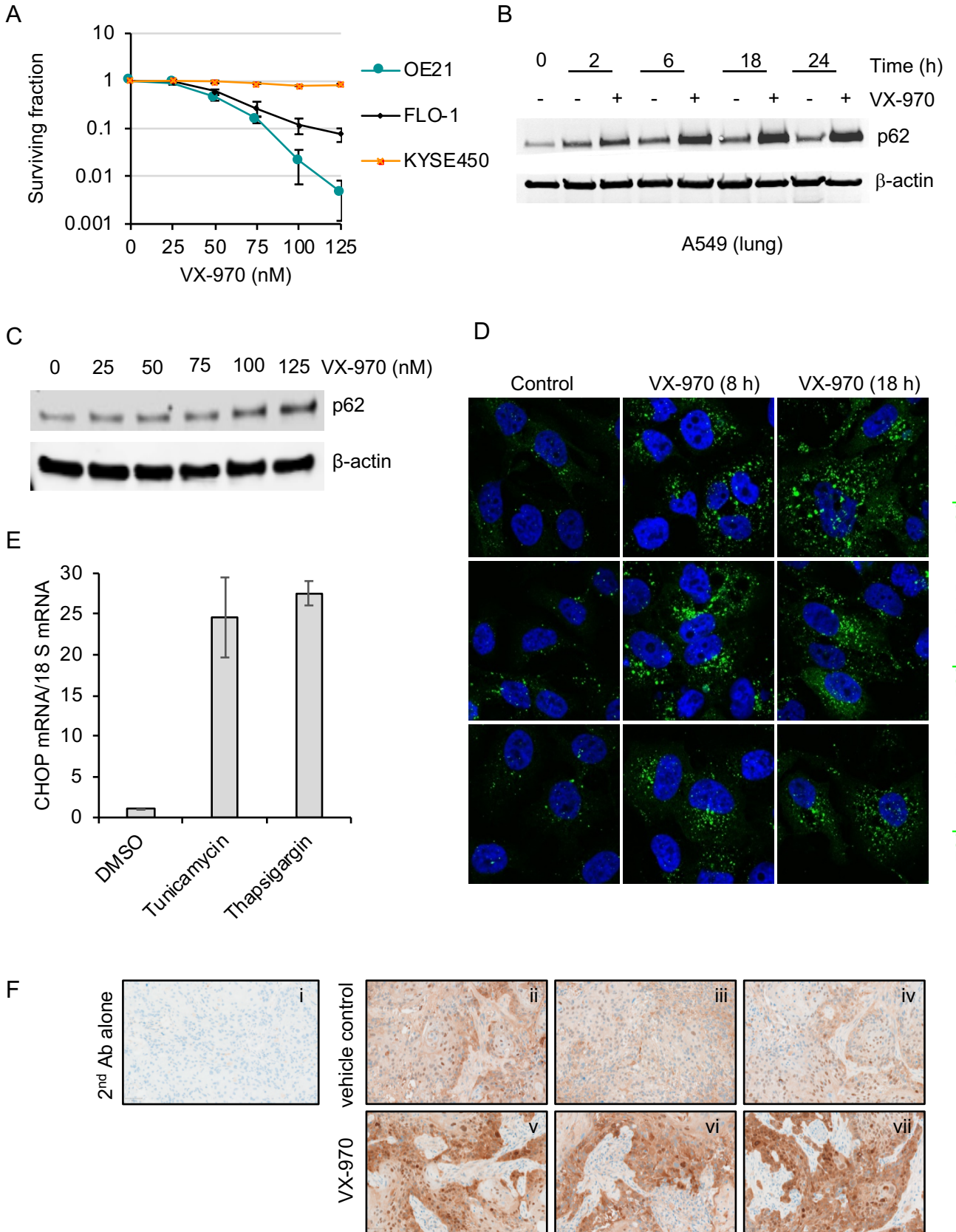
Cells were seeded in 6-well plates and 4 hours later DMSO or VX-970 were added in the range of concentrations (25-125 nM). Cells were allowed to grow for another 1-2 weeks to allow a growth of colonies formed from at least 50 cells each, which were then stained with crystal violet. Data was analysed as described previously (Leszczynska et al., 2016).

#### Supplemental References

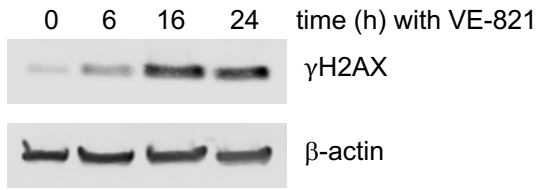
Bencokova, Z., Kaufmann, M. R., Pires, I. M., Lecane, P. S., Giaccia, A. J. and Hammond, E. M. (2009) 'ATM activation and signaling under hypoxic conditions', *Mol Cell Biol*, 29(2), pp. 526-37.

Dobrynin, G., McAllister, T. E., Leszczynska, K. B., Ramachandran, S., Krieg, A. J., Kawamura, A. and Hammond, E. M. (2017) 'KDM4A regulates HIF-1 levels through H3K9me3', *Sci Rep*, 7(1), pp. 11094.

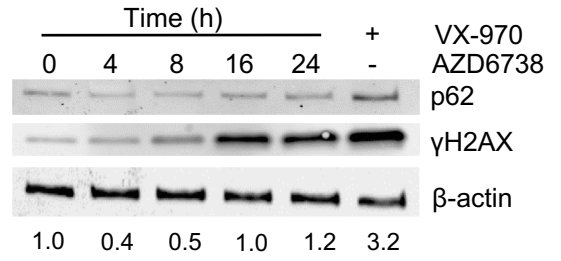
Leszczynska, K. B., Dobrynin, G., Leslie, R. E., lent, J., Boumelha, A. J., Senra, J. M., Hawkins, M. A., Maughan, T., Mukherjee, S. and Hammond, E. M. (2016) 'Preclinical testing of an Atr inhibitor demonstrates improved response to standard therapies for esophageal cancer', *Radiother Oncol*, 121(2), pp. 232-238.



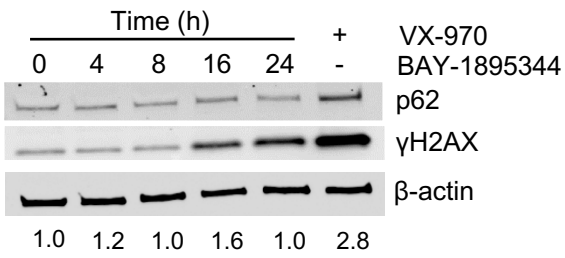
A



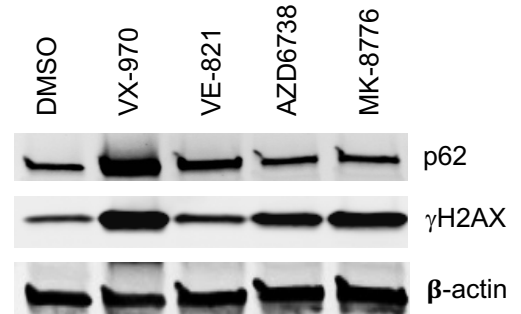
B



C



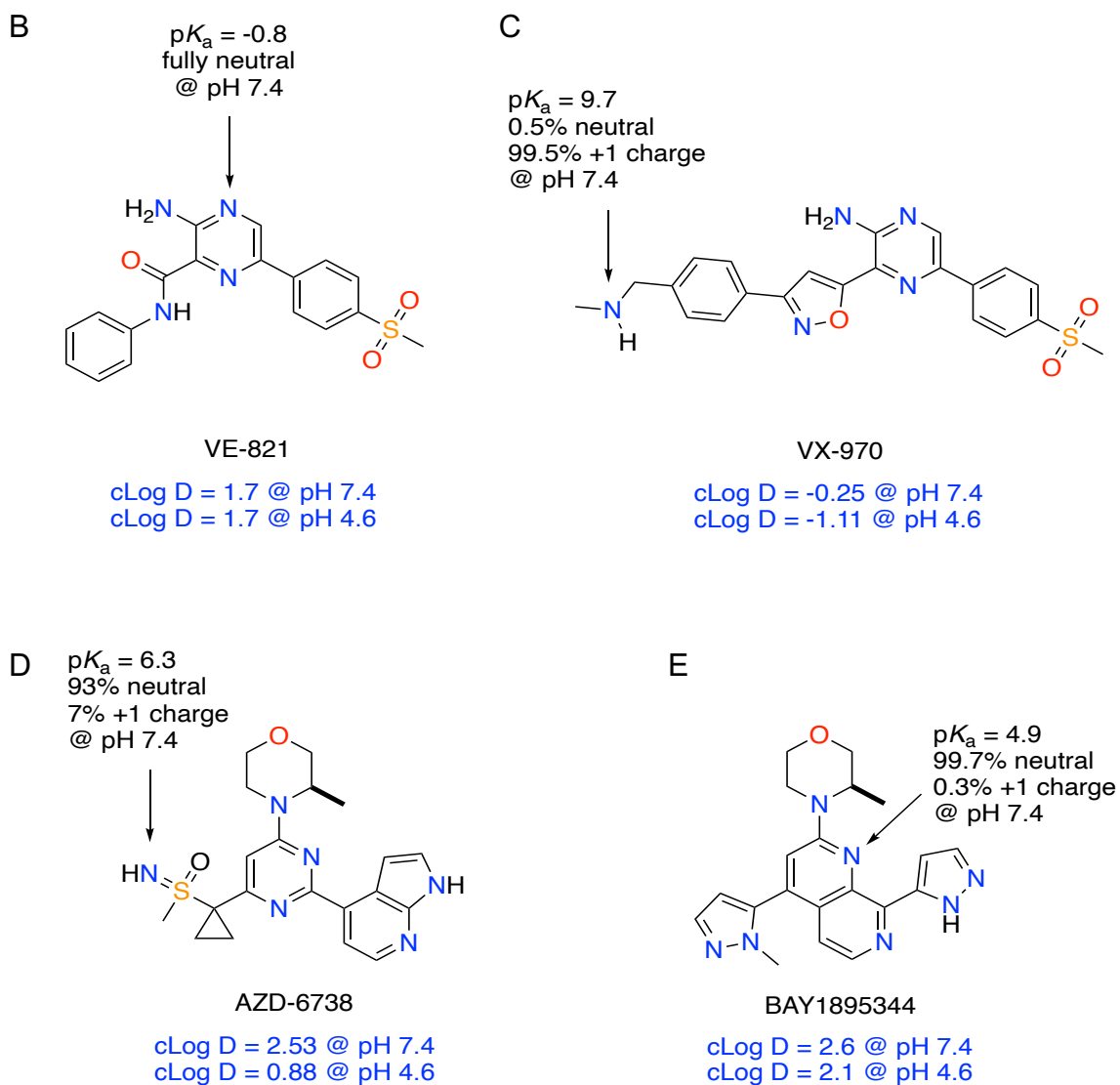
D



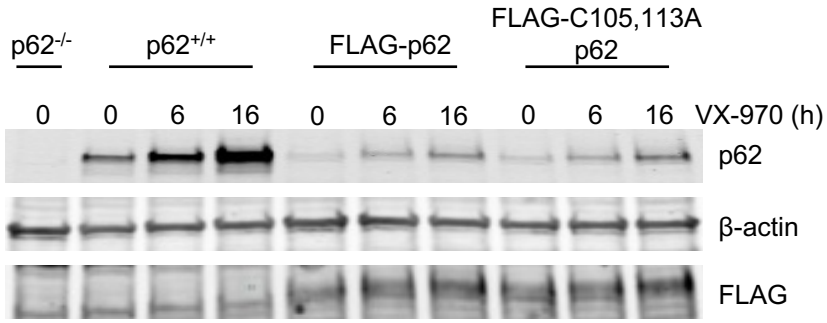
**A**

IC <sub>50</sub>	ATR	ATM	DNA-PK	mTOR
VE-821	17.35 nM (OE21) <sup>1</sup> 13 nM (cell-free) <sup>3</sup>	16 μM (K <sub>i</sub> ) <sup>3</sup>	2.2 μM (K <sub>i</sub> ) <sup>3</sup>	>1 μM (K <sub>i</sub> ) <sup>3</sup>
VX-970	2.30 nM (OE21) <sup>1</sup> 19 nM (HT29) <sup>3</sup>	2.6 μM (PSN-1) <sup>2</sup>	>4 μM <sup>2</sup>	>1 μM <sup>2</sup>
AZD-6738	3.08 nM (OE21) <sup>1</sup> 1 nM (cell-free) <sup>3</sup>			
BAY-1895344	7 nM (cell free) <sup>3</sup>			

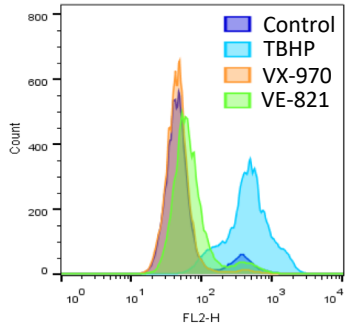
<sup>1</sup> <https://www.cancerrxgene.org> <sup>2</sup> [medchemexpress.com](http://medchemexpress.com) <sup>3</sup> [Selleckchem.com](http://Selleckchem.com)



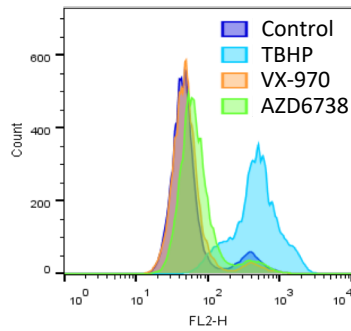
A



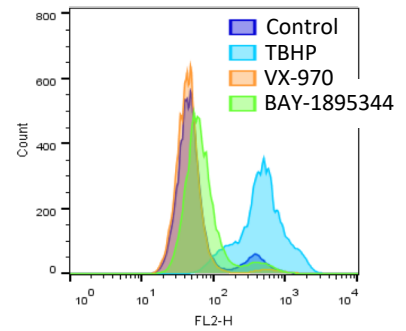
B

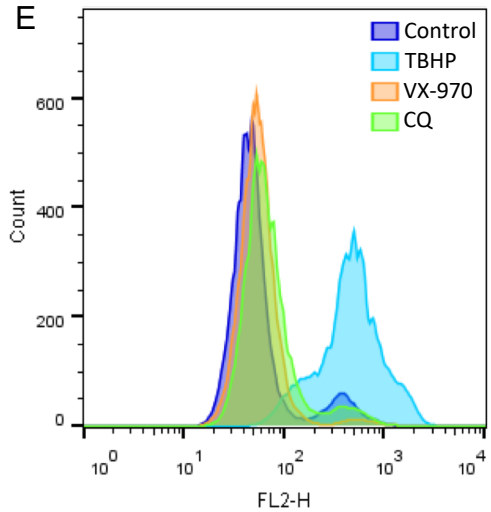
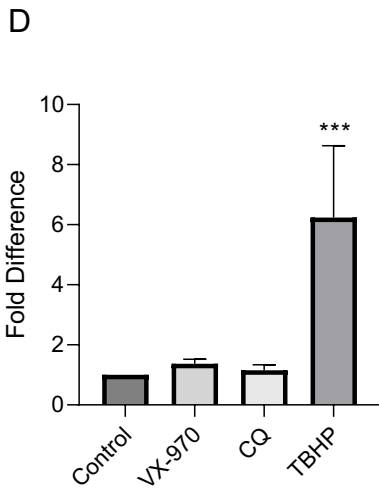
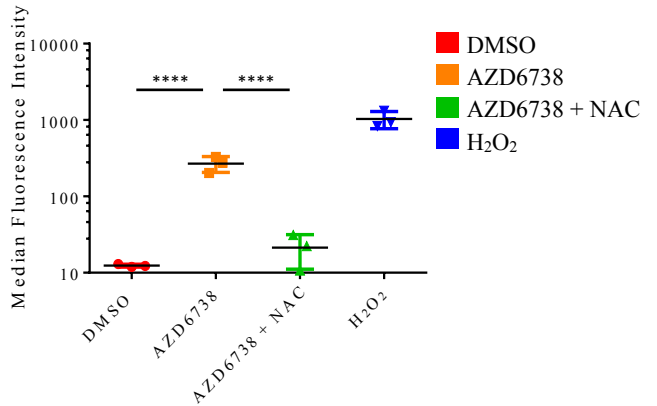
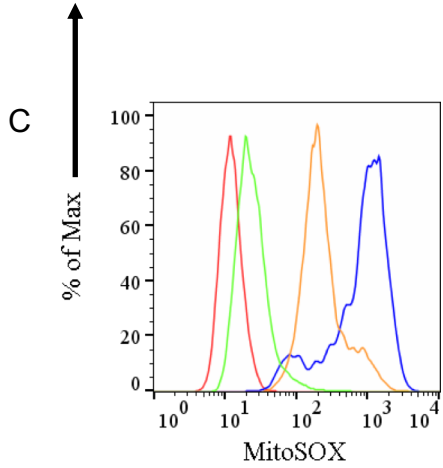
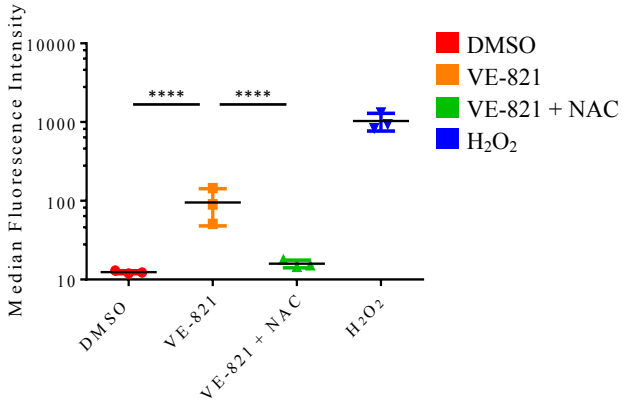
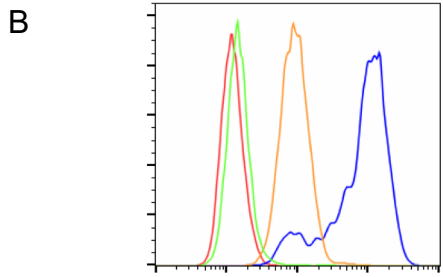
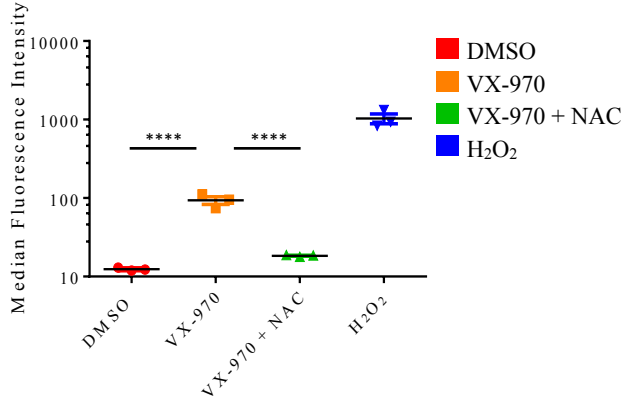
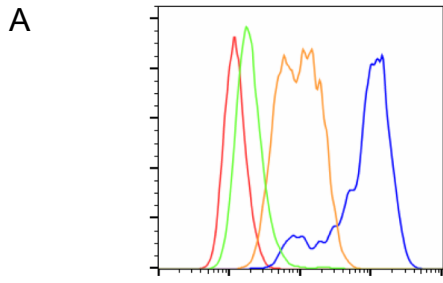


C

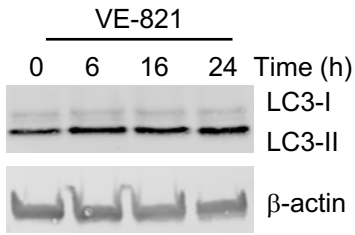


D

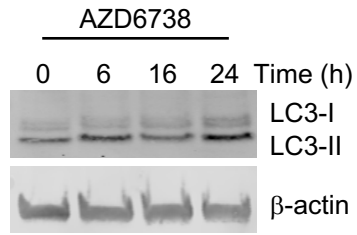




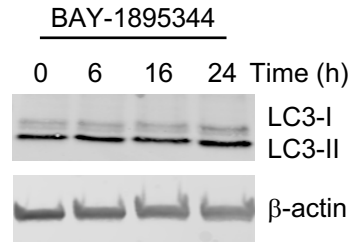
A



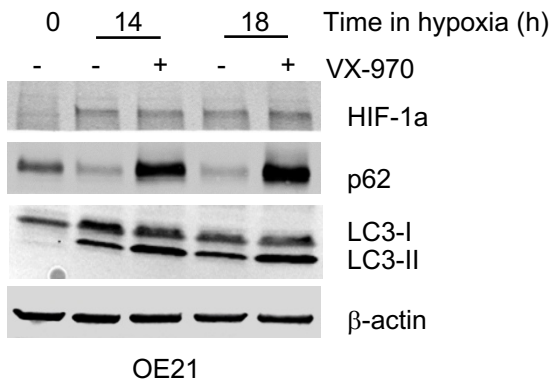
B



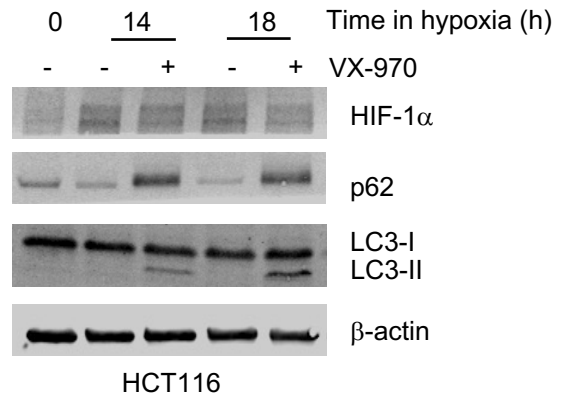
C



D



E



F

